

Absolute emission altitude of pulsars: PSRs B1839+09, B1916+14, and B2111+46

R. M. C. Thomas¹ and R. T. Gangadhara²

¹ National Center for Radio Astrophysics, Pune – 411007, India
e-mail: mathew@ncra.tifr.res.in

² Indian Institute of Astrophysics, Bangalore – 560034, India
e-mail: ganga@iiap.res.in

Received 12 February 2009 / Accepted 12 February 2010

ABSTRACT

Aims. We study the mean profiles of the multi-component pulsars PSRs B1839+09, B1916+14 and B2111+46. We estimate the emission height of the core components, and hence find the absolute emission altitudes corresponding to the conal components.

Methods. By fitting Gaussians to the emission components, we determine the phase location of the component peaks. Our findings indicate that the emission beams of these pulsars have the nested core-cone structures. Based on the phase location of the component peaks, we estimate the aberration-retardation (A/R) phase shifts in the profiles. Due to the A/R phase shift, the peak of the core component in the intensity profile and the inflection point of the polarization angle swing are found to be symmetrically shifted in the opposite directions with respect to the meridional plane in such a way that the core shifts towards the leading side and the polarization angle inflection point towards the trailing side.

Results. We have been able to locate the phase location of the meridional plane and to estimate the absolute emission altitude of both the core and the conal components relative to the neutron star center, using the exact expression for the A/R phase shift given by Gangadhara (2005).

Key words. stars: rotation – pulsars: individual: PSR B1839+09 – pulsars: individual: PSR B1916+14 – pulsars: individual: PSR B2111+46

1. Introduction

Pulsar radio emission is understood to be emitted by the relativistic plasma accelerated along the dipolar magnetic field lines (e.g., Ruderman & Sutherland 1975). Among the various models proposed for pulsar emission, the coherent curvature radiation has turned out to be an effective mechanism for explaining some of the important pulsar radiation properties. The common occurrence of an odd number of components in the mean pulsar profiles has led to the nomenclature of a nested conal structure for the pulsar emission beam (e.g., Rankin 1983a; Rankin 1993). However, Lyne & Manchester (1988) suggested that the emission within the beam is patchy, i.e., the distribution of component locations within the beam is random rather than organized in one or more hollow cones. Also studies by Mitra & Deshpande (1999) indicate that the structure of the pulsar emission beam is more likely to be nested hollow cones. Gangadhara & Gupta (2001, hereafter GG01), and Gupta & Gangadhara (2003, hereafter GG03) showed that the prevalent picture of emission cones axially located around the central core component is a suitable model for explaining the core-cone structure of the pulsar emission beam.

A long-standing question in pulsar astronomy has been the location of the radio emission region in the magnetosphere. In the literature, there are mainly two types of methods proposed for estimating the radio emission altitudes: (1) a *purely geometric method*, which assumes the pulse edge is emitted from the last open field lines (e.g., Cordes 1978; Gil & Kijak 1993; Kijak & Gil 2003); (2) a *relativistic phase shift method*, which assumes that the asymmetry in the conal components phase

location relative to the core is due to the aberration-retardation phase shift (e.g., GG01, Gangadhara 2005, hereafter G05). Both methods have merits and demerits: the first method has an ambiguity in identifying the last open field lines, while the latter is restricted to the profiles in which the core-cone structure can be clearly identified. The emission heights of PSR B0329+54 given in GG01, six other pulsars in GG03 and the revised ones by Dyks et al. (2004, hereafter DRH04) are all relative to the emission height of the core, which is assumed to be zero. However, the core emission is believed to originate from lower altitudes than that of the conal components (e.g., Blaskiewicz et al. 1991; Rankin 1993). Hoensbroech & Xilouris (1997) estimated the emission heights at high frequency radio profiles for a set of pulsars. They suggested that the emission heights at high frequency can set an upper limit for the core emission height.

By assuming a fixed emission altitude across the pulse, Blaskiewicz et al. (1991, hereafter BCW91) presented a relativistic rotating vector model. The results of this purely geometric method are found to be in rough agreement with those of BCW91. However, the relativistic phase shift method clearly indicates that the emission altitude across the pulse window is not constant (GG01; GG03; DRH04; Johnston & Weisberg 2006; Krzeszowski et al. 2009).

By considering the relativistically beamed radio emission in the direction of the magnetic field line tangents, Gangadhara (2004, hereafter G04) solved the viewing geometry in an inclined and slowly rotating dipole magnetic field. A more exact expression for the relativistic phase shift is given in (G05), which also includes the phase shift due to polar cap currents. In the present work, we analyze the mean profiles of PSRs B1839+09

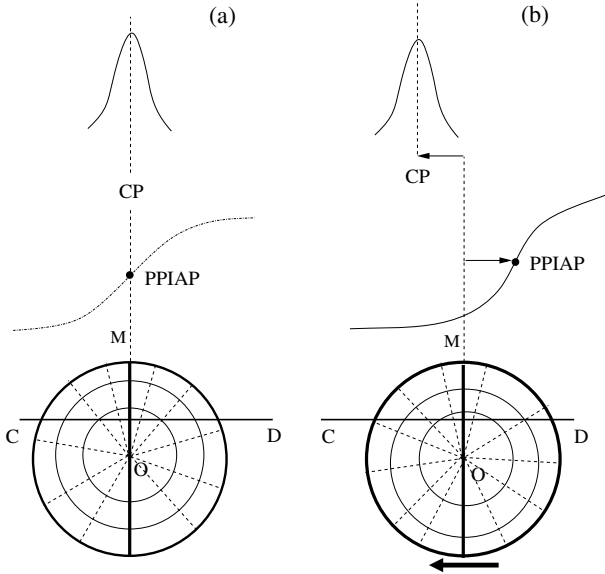


Fig. 1. Schematic diagram showing the A/R phase shift between the core peak (CP) and the polarization position angle inflection point (PPAIP). The panel **a)** for the co-rotating frame, where the phases of PPAIP and CP coincide with that of the meridional plane (M), and **b)** in laboratory frame, due to A/R effects, both the PPAIP and the CP are symmetrically shifted in the opposite directions with respect to M.

and B1916+14 at 1418 MHz, and PSR B2111+46 at 610 MHz and 1408 MHz, to estimate the absolute emission height of the pulse components. In Sect. 2, we give a method for estimating the absolute emission height of pulse components.

2. Method for estimating the absolute emission heights

The work of BCW91 generalized the rotating vector model (RVM) to include the relativistic effects due to rotation. According to their model, the centroid of the intensity profile advances to an earlier phase by $\sim r/r_{LC}$, while the polarization position angle inflection point (PPAIP) is delayed to a later phase by $\sim 3r/r_{LC}$, where r is the radial distance from the center of neutron star and r_{LC} is the light cylinder radius. After estimating the width of the pulse at $\approx 10\%$ intensity level and by fitting the relativistic rotating vector model, they estimated the phase shift between the centroid of the profile and the PPAIP. But the retardation phase shift was ignored in BCW91, as they assumed a constant emission height across the pulse. In GG01, GG03, Johnston & Weisberg (2006) and Krzeszowski et al. (2009) it was shown though that the emission altitude is not constant across the pulse, and hence retardation has to be taken into account while estimating the A/R phase shifts. Further, Dyks et al. (2004) showed that the centroid of the intensity profile advances by $\sim 2r/r_{LC}$ while the PPAIP is delayed by $\sim 2r/r_{LC}$ due to A/R effects with respect to the meridional plane.

By solving the viewing geometry in the dipole magnetic field, Gangadhara (2005) showed that instead of a centroid of intensity profile, the phase shift of the central (core) peak (CP) relative to the meridional plane must be considered for estimating the A/R phase shifts. In the co-rotating (non-rotating) case both core and PPAIP originate from the same phase (meridional plane M, see Fig. 1a). Whereas in the observer (laboratory) frame, the CP shifts to the earlier phase and the PPAIP to the later phase by the same magnitude (see Fig. 1b). Hence to find

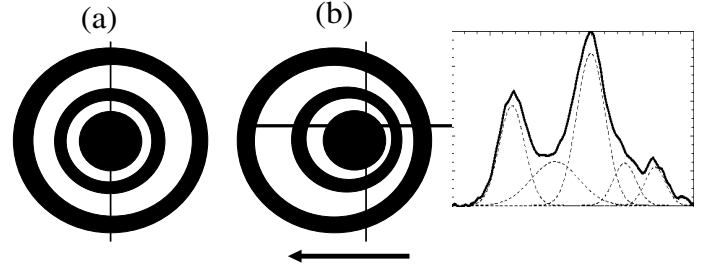


Fig. 2. Schematic diagram to show the probable distribution of emission patterns across the pulsar beam. The beam cross sections as they appear in **a)** the co-rotating frame and **b)** the laboratory frame, where the cones are not coaxial with the central core because of A/R retardation effects. The thick horizontal line represents the direction of the tracing of the line-of-sight across the beam. The resultant intensity profile is shown in the adjoining box. The vertical line denotes the meridional plane, and the thick arrow represents the direction of the pulsar rotation.

the absolute emission height of the profile components including the central (core) component, we adapted the method of G05 to consider the CP instead of the centroid of pulse (BCW91) for estimating the A/R phase shift. It is logical to presume that the aforesaid r should be the same for the origin of the central (core) component and the PPAIP. Or stated otherwise, the phase difference $\Delta\phi'_{CP} = \phi'_{core} - \phi'_{PPAIP} \sim 0$, in the co-rotating frame, where ϕ'_{core} is the phase location of the core peak while ϕ'_{PPAIP} is the phase location of the PPAIP.

As illustrated in Fig. 2, the panel (a) depicts the cross section of the emission region in the co-rotating frame, while panel (b) shows for the same in the observer's frame. The thick arrow represents the direction of the rotation, and the thinner line the sweep of the line-of-sight. The shaded ring-like region represents the nested conal emission regions and the central circle the core emission region. The sweep of the line-of-sight across the depicted region causes the core peak and the PPAIP to be separated by a roughly equal measure ($\sim 2r/r_{LC}$) in opposite directions from the meridional plane (M), as illustrated in Fig. 1. The resultant intensity profile, which characterizes a sum total of emissions after the line-of-sight sweeps across the emission region, is shown in the adjoining box on the right hand side.

3. Application of the method

The implementation of the aforesaid method to estimate the absolute emission height of the core and conal components is described below. We considered the mean profiles of PSRs B1839+09, B1916+14 and B2111+46 for our study, as they exhibit a clearly identifiable core and smooth polarization-position-angle (PPA) swing. We obtained the data of PSRs B1839+09 and B1916+14 from Everette & Weisberg (2001), and those of PSR B2111+46 from EPN data base.

3.1. Longitude of the core peak

We fitted Gaussians to the pulse components to resolve the individual components based on the method developed by Kramer et al. (1994), and the profiles are given in Figs. 3–6. Hence the peak-phase locations of the individual components are resolved. The broken line curves in panel (a) indicate the fitted Gaussians. The phase location of the core peak (ϕ'_{core}) is marked with an arrow and is tabulated in Table 1. The PPA is plotted in panel (b), and the vertical lines mark the fitted region of the curve. The

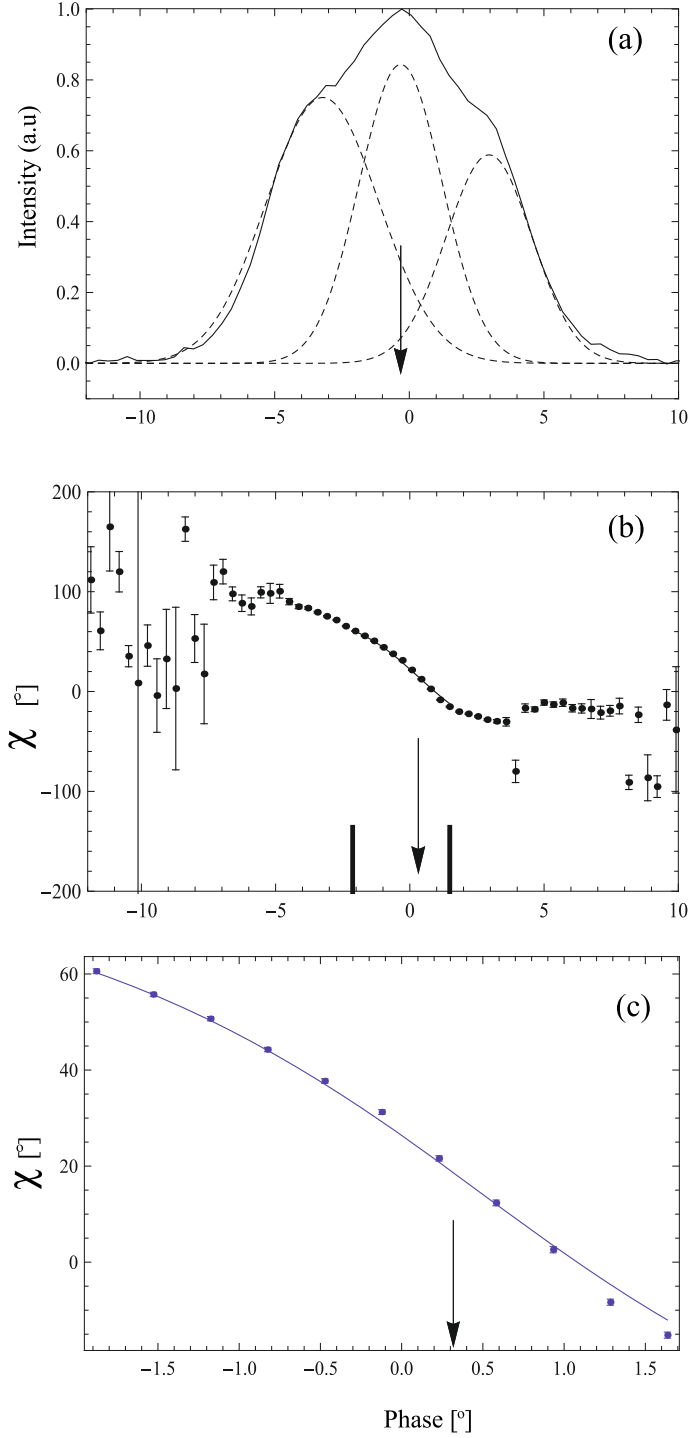


Fig. 3. Intensity profile of PSR B1839+09 at 1418 MHz, fitted with the Gaussians to the sub-pulse components. In panel **a**) the continuous line represents the observed mean profile while the broken line curves represent the fitted Gaussians. The arrow points to the phase of the core peak. In panel **b**) the corresponding polarization angle (χ) is fitted with relativistic RVM curve (BCW91) curve. The arrow points to the phase of inflection point (PPAIP), and the vertical lines mark the region of phase over which the BCW91 curve is fitted. In panel **c**) the zoomed out region demarcated by the vertical lines in panel **b**), is plotted and the arrow points to the PPAIP.

panel (c) shows the zoomed-out region of the PPA within the region of the fit. The arrow points to the PPAIP in both panels (b) and (c).

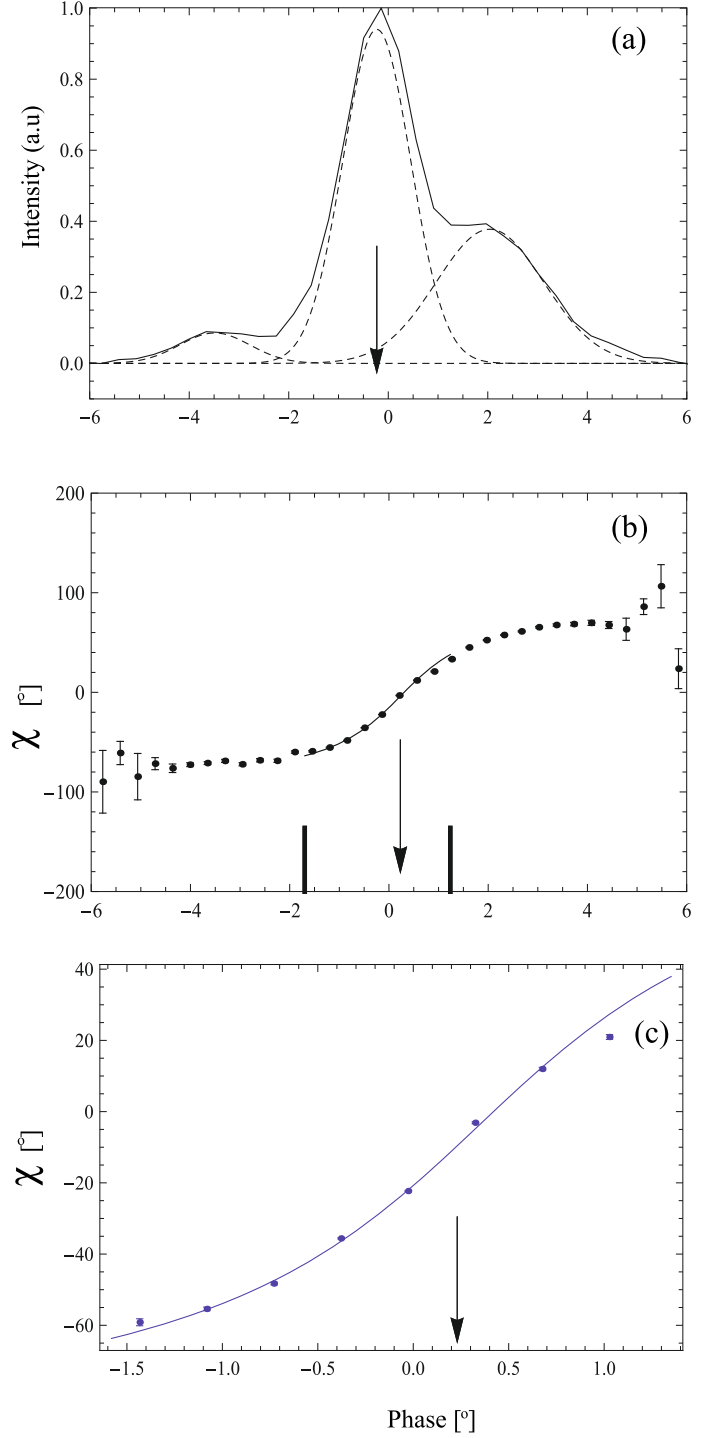


Fig. 4. Intensity profile of PSR B1916+14 at 1418 MHz. See the caption of Fig. 3 for details.

The location of the central component (core) is expected to appear at M for an observer in the co-rotating frame as explained in Sect. 2 and illustrated in Fig. 1a. But for an observer in the laboratory frame, the core emission will be advanced to an earlier phase by $\delta\phi'_{\text{core}} \sim -2 r_{\text{core}}/r_{\text{LC}}$ and the corresponding PPAIP delayed to a later phase by $\delta\phi'_{\text{PPAIP}} \sim 2 r_{\text{core}}/r_{\text{LC}}$, where r_{core} is the emission height of the core. Then the A/R phase shift of the core with respect to M is $\delta\phi'_{\text{core}} = \Delta\phi'/2$, and the parameters related to core emission are given in Table 1. The frequency ν of each data set is given in Col. 2, and the phase shifts $\delta\phi'_{\text{core}}$ and $\delta\phi'_{\text{PPAIP}}$ in Cols. 3 and 4.

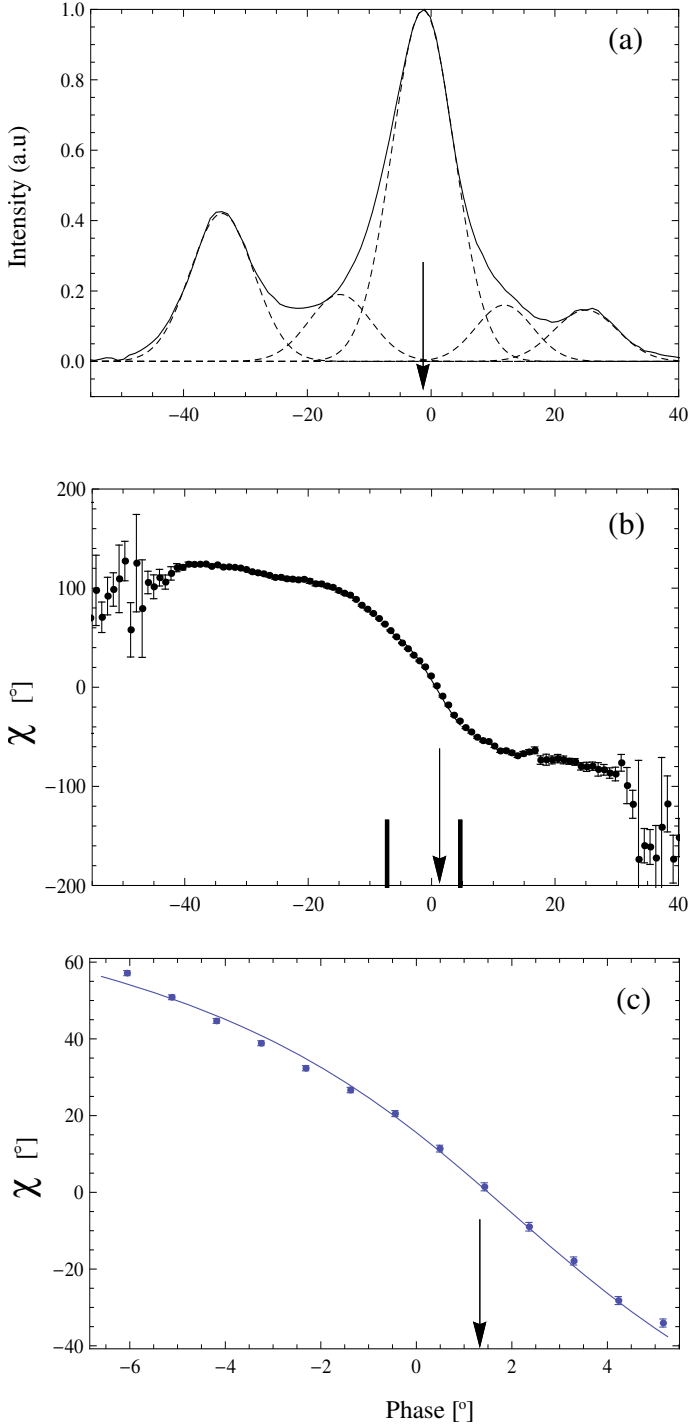


Fig. 5. Intensity profile of PSR B2111+46 at 610 MHz. See the caption of Fig. 3 for details.

3.2. The relativistic RVM fit

We fitted the relativistic RVM (BCW91) to the region of the PPA data, which corresponds to the core emission, the region over which the core polarization is significantly higher than that over the adjacent conal regions. We could see from the profiles that the pulse phase range falling within the full-width-at-half-maximum (FWHM) of the central-fit-Gaussian can clearly bracket out the emissions that dominate the core. The core emission is found to be dominant within 10% intensity levels of the central Gaussian of the 1418 MHz data of PSR B1916+14, and

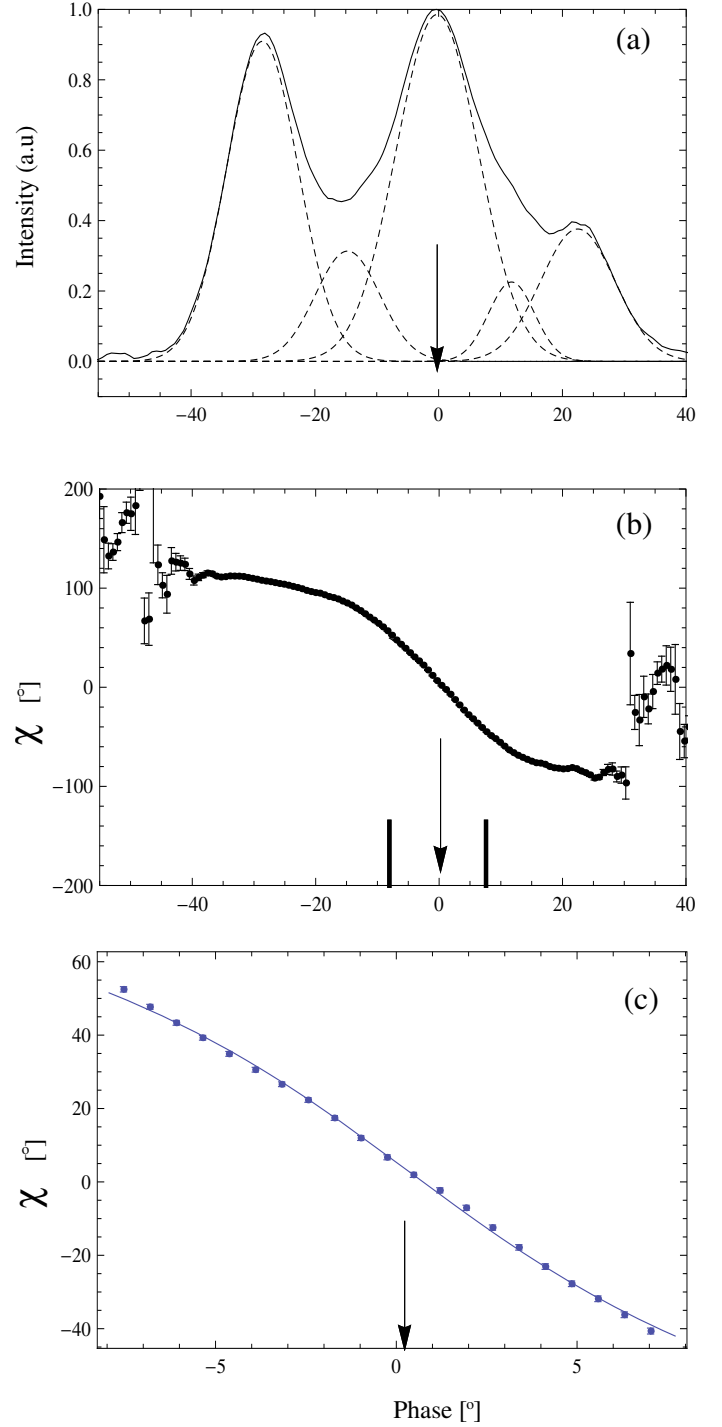


Fig. 6. Intensity profile of PSR B2111+46 at 1408 MHz. See the caption of Fig. 3 for details.

hence we included that region for fitting the BCW91 curve for that profile. Additional reasons for restricting the fit region are discussed in detail in later sections.

3.2.1. Longitude of polarization position angle inflection point

We invoked the guess values for the emission height r and the phase ϕ'_{PPAIP} to fit the BCW91 curve. The polarization angle data, falling within the FWHM of the core, are fitted with a 6th degree polynomial: $\psi(\phi') = a_0 + a_1\phi' + a_2\phi'^2 + \dots$, where a_0, a_1, a_2, \dots are the fit coefficients, and ϕ' is the pulse phase

Table 1. Core emission geometry parameters of PSRs B1839+09, B1916+14 and B2111+46.

Pulsar PSR B (1)	ν (MHz) (2)	$\delta\phi'_{\text{core}}$ ($^{\circ}$) (3)	$\delta\phi'_{\text{PPAIP}}$ ($^{\circ}$) (4)	r_{core} (km) ^a (5)	r_{core} (% r_{LC}) (6)	χ^2 (7)	SR (%) ^b (8)	s/s_{lof} foot value (9)
1839+09	1418	-0.32 ± 0.07	0.32 ± 0.01	50 ± 5	0.28 ± 0.03	102.	100	0.51 ± 0.03
1916+14	1418	-0.23 ± 0.02	0.23 ± 0.01	95 ± 4	0.20 ± 0.01	28.25	94	0.26 ± 0.01
2111+46	610	-1.33 ± 0.02	1.33 ± 0.20	503 ± 38	1.04 ± 0.08	5.7	100	0.13 ± 0.00
	1408	-0.23 ± 0.08	0.23 ± 0.29	83 ± 54	0.17 ± 0.11	2.05	95	0.51 ± 0.17

Notes. ^(a) Emission heights computed using the exact formula (G05). ^(b) The percentage of the standardized residuals (SR) with value of -2 and $+2$.

Table 2. Conal emission geometry parameters of PSRs B1839+09, B1916+14 and B2111+46.

Pulsar PSR B (1)	ν (MHz) (2)	Cone (No.) (3)	ϕ'_L ($^{\circ}$) (4)	ϕ'_T ($^{\circ}$) (5)	$\delta\phi'$ ($^{\circ}$) (6)	Γ ($^{\circ}$) (7)	r (km) ^a (8)	r (% r_{LC}) (9)	s/s_{lof} foot value (10)
1839+09	1418	1	-3.75 ± 0.15	2.96 ± 0.18	-0.39 ± 0.12	4.06 ± 2.30	63 ± 19	0.34 ± 0.10	0.80 ± 0.10
1916+14	1418	1	-3.49 ± 0.05	2.04 ± 0.07	-0.72 ± 0.04	2.63 ± 1.00	299 ± 18	0.63 ± 0.04	0.39 ± 0.01
2111+46	610	1	-14.78 ± 0.45	11.79 ± 0.31	-1.49 ± 0.27	2.85 ± 1.10	581 ± 107	1.20 ± 0.22	0.30 ± 0.02
		2	-33.83 ± 0.21	24.95 ± 0.22	-4.44 ± 0.15	5.87 ± 1.10	1891 ± 64	3.91 ± 0.13	0.35 ± 0.00
	1408	1	-14.70 ± 0.40	11.78 ± 0.34	-1.46 ± 0.27	3.30 ± 1.80	533 ± 97	1.10 ± 0.20	0.37 ± 0.03
		2	-28.47 ± 0.31	22.48 ± 0.34	-2.99 ± 0.23	5.58 ± 1.80	1151 ± 87	2.38 ± 0.18	0.42 ± 0.01

Notes. ^(a) Emission heights computed using the exact formula (G05).

in degrees. We differentiated the fitted polynomial and found the maximum of $|d\psi/d\phi'|$ that gives the guess value of ϕ'_{PPAIP} . In the next step, the PPA data were fitted with the relativistic RVM curve (BCW91) using the following expression

$$\psi_{\text{BCW}} = \psi_0 + \tan^{-1} \left[\frac{\sin \alpha \sin(\Omega t) - 3(r/r_{\text{LC}}) \sin \zeta}{\sin \beta + \sin \alpha \cos \zeta (1 - \cos(\Omega t))} \right], \quad (1)$$

where $\zeta = \alpha + \beta$. The inclination angle of the magnetic axis relative to rotation axis is α , and the impact angle of the line-of-sight relative to the magnetic axis is β . The fitted PPA data are shown in the panel (b) of Figs. 3–6.

The parameter ψ_0 is inserted in the above Eq. (1) in order to offset the possible arbitrary and constant ‘‘vertical shift’’ that the raw PPA data might have. This is due to the arbitrary value of the projection of the rotation axis in the sky plane. Since we are interested in finding r , which is expected to be relatively constant in the region of fit, we assumed it to be independent of ϕ' ($=\Omega t$), and hence it is taken as a fitting parameter. The vertical shift in the raw PPA data, in the first step, was brought closer to zero by finding a trial value for the PPAIP on the vertical axis (ψ_T) from the polynomial fit, and thereafter the data were shifted vertically so that $\psi_{\text{POL}} \rightarrow \psi_{\text{POL}} - \psi_T$, where ψ_{POL} is the observed polarization angle. These PPA data were fitted with Eq. (1) keeping r and ψ_0 as the free parameters; hence allowing two degrees of freedom for the fit function, i.e., allowing the fit function to ‘‘adjust’’ in both the vertical (through the free parameter ψ_0) and horizontal direction (through free parameter r) for a good fit. The fit procedure was repeated consecutively a few times, with the values of r and ψ_0 from the preceding fit as guess values for the final convergent and stable values. Thus ϕ'_{PPAIP} was found from the fit, and the corresponding values are shown in Table 1. The geometric angles α and β were not invoked as fit parameters in Eq. (1) because we used their predetermined (published) values in the BCW91 fit function. We used the values of α and β given by Everette & Weisberg (2001) for PSRs B1839+09 and B1916+14, and for PSR B2111+46 by Mitra & Li (2004, hereafter ML04).

3.3. The longitude of the meridional plane

The CP and PPAIP of the polarization angle appear at M in the co-rotating frame, as indicated by Fig. 1a. But they are symmetrically shifted in opposite directions from M due to the A/R phase shift for an observer in the laboratory frame, as indicated by Fig. 1b. Note that the phase location of M is invariant with respect to the rotation effects, or in other words, both the CP and the PPAIP come closer to M at smaller r , and move away from it at larger r . If ϕ'_{core} and ϕ'_{PPAIP} are the estimated phases of the CP and the PPAIP, then their phase difference ($\Delta\phi'$) is given by $\Delta\phi' = \phi'_{\text{PPAIP}} - \phi'_{\text{core}}$, and the meridional plane M is situated at the mid point between CP and PPAIP. Hence the phase of M is given by $\phi'_M = \phi'_{\text{core}} + (\Delta\phi'/2)$. In Figs. 3–6 the phases are shifted by ϕ'_M , so that M appears at the zero phase and an arrow points to the phase location ϕ'_{PPAIP} in the polarization angle panels (b).

3.4. The A/R phase shift of the core

The location of the central component (core) should appear at M for an observer in the co-rotating frame as explained in Sect. 2. But for an observer in the laboratory frame, the core emission will be advanced to an earlier phase by $\delta\phi'_{\text{core}} \sim -2r_{\text{core}}/r_{\text{LC}}$ and the corresponding PPAIP be delayed to a later phase by $\delta\phi'_{\text{PPAIP}} \sim 2r_{\text{core}}/r_{\text{LC}}$, where r_{core} is the emission height of the core. Then the A/R phase shift of the core with respect to M is $\delta\phi'_{\text{core}} = \Delta\phi'/2$.

3.5. Phase locations of the core and cone component peaks

We found the peak locations of the individual components by fitting Gaussians to the mean profiles of the three pulsars. As mentioned in Sect. 3.3, the data were shifted by ϕ'_M so that M appears at zero phase. Because the A/R effects are absent in the co-rotating frame, the conal components are expected to be symmetrically located on either sides of meridional plane as indicated by Fig. 2a. But in the laboratory frame, the cones are advanced to an earlier phase due to the A/R effects and are hence

asymmetric with respect to the core location as indicated by Fig. 2b. The meridional plane M is taken to be at the zero phase, and the measured phases are, therefore, the absolute phases with respect to M. Accordingly the estimated emission heights are the absolute emission altitudes with respect to the center of the neutron star.

Let ϕ'_L and ϕ'_T be the peak locations of the conal components on the leading and trailing sides of a pulse profile, respectively. Then, using the following equations, we estimate the A/R phase shift ($\delta\phi'$) of the cone center with respect to M, and the phase location (ϕ') of the component peaks in the absence of the A/R phase shift, i.e., in the co-rotating frame (see Eq. (11) in GG01):

$$\delta\phi' = \frac{1}{2}(\phi'_T + \phi'_L), \quad \phi' = \frac{1}{2}(\phi'_T - \phi'_L). \quad (2)$$

4. The absolute emission heights

4.1. Emission height of the core

The core emission height was computed by using the $\delta\phi'_{\text{core}}$ in the expression for the A/R phase shift given by G05 (see Eq. (45)). The parameters related to the core emission are given in Table 1. In Col. 6 the emission heights are given as a percentage of the light cylinder radius r_{LC} . It shows that the core emission in the radio band occurs over a range of altitude spanning from 0.2 to 1 per cent of the light cylinder radius. The radio frequency ν of each data set is given in Col. 2, and the phase shifts $\delta\phi'_{\text{core}}$ and $\delta\phi'_{\text{PPAIP}}$ in Cols. 3 and 4, respectively. The values of χ^2 and the standard residuals obtained are given in Cols. 7 and 8, respectively. The foot location of magnetic field lines on the polar cap relative the magnetic axis are given in Col. 9.

4.2. Emission height of the cones

We found the emission height of the cones based on the procedure that is described in Sect. 3.5. In Col. 3 of Table 2 we have given the cone numbers and the peak locations of the conal components on the leading and trailing sides in Cols. 4 and 5, respectively. The conal components are believed to arise from the nested conal emissions (Rankin 1983a,b, 1990, 1993), which along with the central core emission make up the pulsar emission beam. In Col. 6 of Table 2, we have given the values of $\delta\phi'$. In general it increases in magnitude from the innermost cone to the outer cone. The half-opening angle Γ (see Eq. (7) in G04) of the emission beam is given in Col. 7. Using the exact formalism for the A/R phase shift (see Eq. (45) in G05), we computed the emission heights and show them in Col. 8. Their percentage values in r_{LC} are given in Col. 9. In Col. 10, we give the normalized co-latitude s/s_{lof} of the foot field lines on the polar cap, which are associated with the component emissions. Due to the relativistic beaming and restrictions owing to geometry, we find that the observer tends to receive the emissions from open field lines, which are located in the foot locations ranging from (approximately) 0.1 (Table 1) to 0.8 (Table 2) on the polar cap.

4.3. PSR B1839+09

By fitting three Gaussians to the mean intensity profile of PSR B1839+09 we have identified three sub-pulse components: a central component and a pair of outer components flanking the central one. By invoking the picture of a nested cone structure we infer that the outer pair of components corresponds to a conal emission. The inner component might be due to emissions close

to the magnetic axis or because of the ‘‘grazing-cut’’ of the line-of-sight with an inner ring of emission. The point of emission for the central component should fall in the meridional plane M in the co-rotating frame of the pulsar in either of the cases. We clearly identified the phase locations for the PPAIP and the CP relative to the meridional plane M for PSR B1839+09. The absolute emission heights estimated for the core and conal component are given in Tables 1 and 2, respectively. The emission heights of the central (core) component and cone are found to be ~ 50 km and ~ 60 km, respectively.

4.4. PSR B1916+14

By fitting Gaussians to the intensity profile, we could identify three sub-pulse components: a central component and a pair of outer components flanking the central one. We clearly identified the phase locations of the PPAIP and the central peak, and found the phase of meridional plane M. The absolute emission heights, estimated for the central (core) and conal components, are given in Tables 1 and 2. The emission heights of the central component and the cone are estimated to be ~ 100 km and ~ 300 km, respectively.

4.5. PSR B2111+46

It is a well-studied pulsar. By fitting Gaussians to its intensity profiles at frequencies 610 MHz and 1408 MHz, we could identify five sub-components: a central (core) component, a pair of inner components and a pair of outer components. Our values of the phase locations of the component peaks are in close agreement with the ones given by Zhang et al. (2007) for PSR B2111+46. One can guess at the presence of two inner components hidden between the core and the outer components even by visual inspection. These two hidden components were detected in the previous work of GG03 in the 333 MHz single pulse data. The absolute emission heights estimated for the core and the cones are given in Tables 1 and 2. The core emission height is found to be ~ 500 km at 610 MHz and ~ 80 km at 1408 MHz. It has been reported in ML04 that the widths of the core tend to show a significant frequency evolution in their chosen set of six pulsars, and hence they argued that the core emission does not come from the stellar surface. However, we need to consider more high quality data sets at different frequencies to see the frequency evolution of the core emission height, and whether it follows any radius-to-frequency mapping.

5. Results and discussions

Based on the A/R method, we estimated the absolute emission height of the core as well as cones in three pulsars: PSRs B1839+09, B1916+14 and B2111+46. Though this method is based on the existing standard models in literature, the combination of the A/R phase shift and the delay-radius relation of BCW91 for estimating the core height is novel.

The geometrical method, involving a comparison of the measured pulse widths with geometrical predictions from dipolar models, is believed to yield absolute emission heights. However, the estimation of emission height, using the geometrical method, is based on the assumption that the pulse edges originate from the last open field lines of the polar cap. In general, the edge of the on-pulse region may not originate from the last open field line, and hence the assigning of the edges of the intensity profile to the last open field lines can be misleading. For example, the

range of magnetic foot-colatitude for field-lines that are associated with components in PSR B2111+46 are in the range from $S/S_{\text{lof}} \sim 0.13$ to 0.5, whereas the last open field line is at 1. This means that the boundary of the active region of emission can lie anywhere from ≈ 0.5 to 1.

According to DRH04, the A/R phase shift advances the centroid of the intensity profile to an earlier phase by $\delta\phi'_c = 2r_{\text{lof}}/r_{\text{LC}}$, while the PPAIP is delayed to a later phase by $\delta\phi'_{\text{PPAIP}} \sim 2r_{\text{core}}/r_{\text{LC}}$, where r_{lof} is the emission height from the last open field-line and r_{core} is the emission height of the core. Then $\Delta\phi' = 2(r_{\text{lof}} + r_{\text{core}})/r_{\text{LC}}$, and the emission height $r = r_{\text{LC}} \Delta\phi'/4 = (r_{\text{lof}} + r_{\text{core}})/2$, gives only an average of the emission height for the core and the pulse edge, which is far from the true value. This emission height cannot represent any specific pulse sub-component of the profile, and can be misleading in cases where r_{lof} and r_{core} are significantly different. Further more, this will introduce large systematic errors in the emission heights estimated from geometrical methods, due to the aforesaid assumption of identifying the last open field lines with the pulse edges.

Rankin (1983a) has argued that the pulsar emission cones are quasi-axial, i.e., the conal components are not exactly axially located with respect to the magnetic axis. Mitra & Deshpande (1999) have suggested that the pulsar emission beams are nearly circular in the aligned configuration ($\alpha \sim 0^\circ$) and change to elliptical in the orthogonal configuration ($\alpha \sim 90^\circ$). The majority of the pulsar observations indicate that the beam geometry is likely to be nested cones, distributed in a nearly non-coaxial fashion about the magnetic axis. A likely case is that the cones, which are coaxial in the co-rotating frame, will appear non-coaxial in the laboratory frame because of the A/R phase shifts (GG01; GG03).

In the works GG01 and GG03, the emission height of the core was neglected by assuming that it is considerably smaller than that of the components. However, we find that the emission height of the core is quite significant and cannot be neglected in comparison to the emission height of the components. We identify the meridional plane M as being located at the mid point between the centroid of the intensity profile and the PPAIP, owing to the A/R effects. By recognizing this, we were able to estimate the absolute emission heights of both the core and the conal components.

As mentioned before, we restricted the region of the fit of the BCW91 (relativistic RVM) curve to the section of the PPA data falling within the FWHM of the core component for estimating the core emission height, and the justification for doing so is given now. The expression for the BCW91 was derived by assuming that the emission altitude across the active region of the pulse profile is a constant. Thus in a BCW91 fitting, a single r value was taken to characterize the emission height of the full region of the PPA data. But later observational results (e.g., GG01; GG03) established that the emission altitude corresponding to the subpulse components in multi-component profiles spans over a large range of emission heights. This elicits the fact that in multi-component profiles the r , found by fitting the BCW91 curve to the full PPA region of the active profile, might give an emission altitude that can be significantly different from those obtained from the A/R method for the subpulse components.

The best-fit value of r in the BCW91 model, which is the weighted average of r_i that characterize the emission height at each point of pulse phase, is given by Eq. (C.8) in Appendix C. Hence a single value of r found from the BCW91 fit cannot be closer to the true emission height corresponding to the core or

cone peak if r_i varies significantly within the region of the fit. For example, one can compare the emission altitudes in our Tables 1 and 2 with those given in Table 3 of ML04 for PSR B2111+46. It can be surmised that a single value of r cannot characterize the emission altitude across the entire active region of a multi-component profile.

We can think of two viable alternatives in this scenario: either (1) adapt or modify the BCW91 formulation for a variable emission altitude r (Dyks 2008) or (2) fit the BCW91 curve for regions of the PPA profile having a relatively constant value of r . We prefer the latter alternative to evade the modification of the theory behind the BCW91 model. Here we note that α and β are not invoked as fit parameters; instead we used their published values in Eq. (C.1). This is expected to further reduce the ambiguity of the fit results and to aid in counteracting an obvious disadvantage in this “restricted” fit method, i.e., having a reduced number of fitted PPA data points than a fit for the “full range” of PPA data. It is remarkable that some of the fit statistics (e.g., reduced χ^2) given in Table 1 reveal that the present method of fitting is comparable (in a few cases even better) to the existing ones in the literature (e.g., compare the χ^2 value given in Table 1 with Table 2 of ML04 for PSR B2111+46). We estimated the standardized residuals (SR) and found the percentage of SR that falls within -2 and $+2$ as given in Col. (8) of Table 1. As it is known, a good fit is expected to have a threshold 95% of the standardized residuals to fall within -2 and $+2$. Several previous works found that α and β are highly covariant in PPA fits (e.g., Everette & Weisberg 2001). But this covariance of α and β with the r parameter was not mentioned by any of them. The fit statistics do not reveal any significant covariance of α and β with r . This gives us a further clue for finding the r parameter without invoking a concurrent fit for α and β (see Appendix A for the fitting procedure).

Owing to the extreme difficulties encountered in determining α and β through RVM fitting, a larger range of PPA data have always been preferred for a better fit (e.g., Everette & Weisberg 2001). The justification for doing so is that α and β must remain constant throughout the entire PPA profile. But in the present scenario, as described earlier, the selection of a large range of PPA data for fitting does not always translate into a better estimation of r because of the variation of the emission height with pulse phase. So, owing to all of the above said reasons we restrict the fit of the BCW91 curve to the PPA profile, falling around the core component, which is expected to yield an emission altitude characterizing the core height.

A section of inner cones often lapses over the core as is seen in the Gaussian fits (panel (a) of Figs. 3–6) of the total intensity profiles. The inner cones may contribute to the core polarization near the edges of pulse phase of the FWHM region that we bracketed. Hence the PPA corresponding to the bracketed region will be “contaminated” by the adjacent conals, and this has to be accounted for. We estimated and accounted for the error induced because of this effect in the estimation of the core emission heights (see Appendices B and C).

The possibility that the A/R phase shift may be reduced by the rotational distortion of the magnetic field line due to a sweep-back of the vacuum dipole magnetic field lines has to be considered. The sweep-back of dipole magnetic field lines was first treated in detail by Shitov (1983). Further, Dyks & Harding (2004) investigated the rotational distortion of pulsar magnetic field by making the approximation of a vacuum magnetosphere. For $\phi' = 30^\circ$, $\beta = -1.6^\circ$ and $\alpha = 14^\circ$ we computed the phase shift $\delta\phi'_{\text{mfsb}}$ due to the magnetic field sweep-back (Dyks & Harding 2004; also see Eq. (49) in G05). It is found to

be <0.0001 rad for $r/r_{LC} \leq 0.06$, which is much smaller than the aberration, retardation and polar cap current phase shifts in PSR B2111+46. Hence we neglect the magnetic field sweep-back effect.

The field-aligned polar-cap current does not introduce any significant phase shift into the phase of the PPAIP. But it introduces a positive offset into the PPA, though it roughly cancels due to the negative offset by aberration (Hibschman & Arons 2001). The phase shift of pulse components due to the polar cap current was estimated recently by G05, and found to be quite small compared to the A/R phase shift.

6. Summary

We analyzed the mean profiles of PSRs B1839+09 and B1916+14 at 1418 MHz, and those of B2111+46 at 610 MHz and 1408 MHz. The phase of the peak of central component (core) and that of the polarization position angle inflection point are symmetrically shifted in the opposite directions with respect to the meridional plane due to A/R effects. By recognizing this, *we were able to locate the phase of the meridional plane and to estimate the absolute emission altitudes of the core and the conal components relative to the center of the neutron star.* We used the exact expression for the phase shift given recently by G05. In all the cases we found that the core emission occurs at a relatively lower altitudes than the conal emissions. It is also interesting to note that the core emission at different frequencies in PSR B2111+46 falls in a range of altitude of 80 km at 1408 MHz to about 500 km at 610 MHz. It is clear that the low frequency emission comes from a higher height than that at high frequency. However, to confirm whether the core emission heights also obey any radius-to-frequency mapping demands the recursive analysis with high quality multi-frequency data. We plan to employ the methods described in this paper for the study of a few other pulsars with high quality data.

Acknowledgements. We thank Joel Weisberg for providing the data of PSRs B1839+09 and B1916+14 at 1418 MHz. We used the data available on EPN archive maintained by MPIfR, Bonn, and thank all the observers who have made their data available on the EPN data base. We thank Yashwant Gupta for the helpful comments.

Appendix A: Estimation of $1\sigma_\Psi$

We apply the standard methods of statistics for fitting the observed data with the model. For fitting the PPA data with the BCW91 curve we define the reduced χ^2 as

$$\chi^2 = \sum_i^N \left[\frac{\Psi_{\text{POL}}(\phi'_i) - \Psi_{\text{BCW}}(\phi'_i)}{\sigma_\Psi(\phi'_i)} \right]^2, \quad (\text{A.1})$$

where Ψ_{POL} is the observed polarization angle and Ψ_{BCW} is the model (BCW91) value at the discrete rotation phase ϕ'_i , and N is the number of data points. Minimization of χ^2 gives the best fit. We use Mathematica version 7 for the fitting and other calculations that ensue therewith.

For profile regions with a very high value of L/σ_1 , i.e., for $L/\sigma_1 \gg 10$, the σ_Ψ is taken as

$$\sigma_\Psi = \frac{\sqrt{U^2 \sigma_Q^2 + Q^2 \sigma_U^2}}{2L}, \quad (\text{A.2})$$

where σ_Q and σ_U are the RMS values of the off-pulse Q and U Stokes parameters, respectively. The parameter $L = \sqrt{Q^2 + U^2}$

represents the linear polarization and σ_1 is the standard deviation of total intensity in the off-pulse region. Though the measurements of U and Q around their true values are normally distributed, the PPA measurements are not similarly distributed at the intermediate values of L/σ_1 . Hence the form of σ_Ψ as given above is not appropriate in this regime. The appropriate distribution function that characterizes the Ψ distribution is discussed in detail by Naghizadeh-Khouei & Clarke (1993). The application of their scheme is discussed by Everette & Weisberg (2001); we follow their method for finding the σ_Ψ for the PPA data points. The probability distribution function of the measured position angle Ψ around a true value Ψ_{true} is given by Naghizadeh-Khouei & Clarke (1993) as

$$G(\Psi; \Psi_0, P_0) = \frac{1}{\sqrt{\pi}} \left(\frac{1}{\sqrt{\pi}} + \eta_0 e^{\eta_0^2} (1 + \text{erf}(\eta_0)) \right) e^{-\frac{\Psi^2}{2}}, \quad (\text{A.3})$$

where $\eta_0 = (P_0/\sqrt{2}) \cos[2(\Psi - \Psi_{\text{true}})]$, $P_0 = L_{\text{true}}/\sigma_1$, erf is the error function and L_{true} is the unbiased linear polarization found from the measured linear polarization. Hence the $1\sigma_\Psi$ confidence level in the PPA is found out by adjusting the limits of integration and fixing $\Psi_{\text{true}} = 0$,

$$\int_{-1\sigma_\Psi}^{1\sigma_\Psi} G(\Psi; P_0) d\Psi = 62.86\%. \quad (\text{A.4})$$

We set up a table of the integration values of the integral against a series of discrete P_0 values and the $1\sigma_\Psi$ levels at integral value of 0.6286 are found by interpolation.

Appendix B: Polarization angle Ψ : contribution from the adjacent component to the core

The polarization angle Ψ is defined as

$$\Psi = \frac{1}{2} \tan^{-1} \left(\frac{U}{Q} \right). \quad (\text{B.1})$$

Defining

$$U = U_0 + U_1, \quad (\text{B.2})$$

$$Q = Q_0 + Q_1, \quad (\text{B.3})$$

$$L = \sqrt{U^2 + Q^2}, \quad (\text{B.4})$$

$$L_0 = \sqrt{U_0^2 + Q_0^2}, \quad (\text{B.5})$$

where U_1 and Q_1 are taken as sufficiently small, Ψ can be a series expanded up to the first order in U_1 and Q_1 as

$$\Psi \simeq \Psi_0 + \Delta\Psi, \quad (\text{B.6})$$

$$\Psi_0 = \frac{1}{2} \tan^{-1} \left(\frac{U_0}{Q_0} \right), \quad (\text{B.7})$$

$$\Delta\Psi = \frac{1}{2} \frac{Q_0 U_1 - U_0 Q_1}{U_0^2 + Q_0^2}. \quad (\text{B.8})$$

The expression for $\Delta\Psi$ may be approximated as

$$\Delta\Psi \simeq \frac{1}{2} \frac{Q U_1 - U Q_1}{L^2}, \quad (\text{B.9})$$

provided U_1 and Q_1 are sufficiently small, so that $L_0 \simeq L$.

We use the above expressions for estimating the contribution to Ψ from the adjacent conal components. The suffix ‘‘1’’ indicates the U and Q contribution solely from the inner cone, while

the suffix ‘‘0’’ indicates the pure core contribution for the same. We employ approximations to find the value of U_1 and Q_1 .

Since the total intensity of an inner conal component can be fitted with a Gaussian, we make an assumption that the $U_1(\phi')$ and $Q_1(\phi')$ also follow a Gaussian shape within the adjacent conal component. Thus

$$U_1(\phi') = U_{1(\max)} \exp\left(-\frac{(\phi'_{\max} - \phi')^2}{\sigma_\phi^2}\right) \quad (\text{B.10})$$

and

$$Q_1(\phi') = Q_{1(\max)} \exp\left(-\frac{(\phi'_{\max} - \phi')^2}{\sigma_\phi^2}\right), \quad (\text{B.11})$$

where σ_ϕ is the width and ϕ'_{\max} is the peak phase of the inner conal component (same as the corresponding Gaussian for the total intensity), while $U_{1(\max)}$ and $Q_{1(\max)}$ are the peak values of U_1 and Q_1 , respectively. The total intensity of the inner cone at phase ϕ'_{int} , where the Gaussians corresponding to the core and outer cone intersect, will have the minimum. Hence the values of $U_1(\phi'_{\text{int}})$ and $Q_1(\phi'_{\text{int}})$ may represent approximately the true values of U_1 and Q_1 for the inner-cone at ϕ'_{int} . By using Eqs. (B.10) and (B.11) we can write

$$U_{1(\max)} = U_1(\phi'_{\text{int}}) \exp\left(\frac{(\phi'_{\max} - \phi'_{\text{int}})^2}{\sigma_\phi^2}\right), \quad (\text{B.12})$$

$$Q_{1(\max)} = Q_1(\phi'_{\text{int}}) \exp\left(\frac{(\phi'_{\max} - \phi'_{\text{int}})^2}{\sigma_\phi^2}\right). \quad (\text{B.13})$$

Using Eqs. (B.12) and (B.13), we can find $U_1(\phi')$ and $Q_1(\phi')$, and hence the $\Delta\Psi(\phi')$ is estimated within the bracketed region of PPA.

Note: The PSR B1839+09 has practically no contribution of polarization from the adjacent conals to the bracketed core region. Hence this analysis is not performed for it. The $U_{1(\max)}$ and $Q_{1(\max)}$ for PSR B1916+14 are the values at the peak phases of the adjacent cones and are directly found from the profile data. So, Eqs. (B.12) and (B.13) are not applicable for it. Hence the above-said analysis is done for the profiles of PSR B2111+46 only.

Appendix C: Determination of the r parameter: correcting for adjacent conal contribution

Here, we explain the scheme of the determination of r and $\delta\phi'_{\text{PPAIP}}$ using the BCW91 method with predetermined values of α and β . Consider the expression for the polarization angle given in BCW91:

$$\psi_{\text{BCW}}(\phi_i) = \tan^{-1} \left[\frac{\sin \alpha \sin \phi_i - 3(r/r_{\text{LC}}) \sin \zeta}{\sin \beta + \sin \alpha \cos \zeta (1 - \cos \phi_i)} \right]. \quad (\text{C.1})$$

Here define χ^2 as

$$\chi^2 = \sum_i^N \left[\frac{\tan[\psi_{\text{POL}}(\phi'_i)] - \tan[\psi_{\text{BCW}}(\phi'_i)]}{\sigma_{\tan \psi}(\phi'_i)} \right]^2, \quad (\text{C.2})$$

where $\sigma_{\tan \psi}(\phi'_i) = \tan[\sigma_\psi(\phi'_i)]$, $\sigma_\psi(\phi'_i)$ is the 1σ error determined by using the Naghizadeh-Khouei & Clarke (1993) method (A). The definition of χ^2 as given in Eq. (C.2) is slightly different from that used in the fitting, and this is meant exclusively for an explanatory purpose. Using the χ^2 of this form

makes it easy to derive the following expressions for the r parameter from the BCW91 model. The form of χ^2 that is used in the actual fitting is given in Appendix A (Eq. (A.1)), and the method of correction for the adjacent conal contribution is briefly given at the end of this section.

By minimizing the χ^2 with respect to the parameter r , we can write

$$\frac{d\chi^2}{dr} = 2 \sum_i^N \left(\frac{\tan(\psi_{\text{POL}}(\phi'_i)) - \tan(\psi_{\text{BCW}}(\phi'_i))}{\sigma_{\tan \psi}(\phi'_i)} \right) \times \frac{d}{dr} \tan(\psi_{\text{BCW}}(\phi'_i)) = 0.$$

By substituting for $\tan(2\psi_{\text{BCW}}(\phi'_i))$, we obtain

$$r = \frac{r_{\text{LC}}}{3} \sum_i^N \frac{F(\phi'_i) F_1(\phi'_i)}{\sigma_{\tan \psi}^2(\phi'_i)} \bigg/ \sum_i^N \frac{\sin \zeta F^2(\phi'_i)}{\sigma_{\tan \psi}^2(\phi'_i)}, \quad (\text{C.3})$$

where

$$F_1(\phi'_i) = \frac{\sin \alpha \sin \phi'_i}{\sin \beta + \sin \alpha \cos \zeta (1 - \cos \phi'_i)} - \tan(\psi_{\text{POL}}(\phi'_i)) \quad (\text{C.4})$$

and

$$F(\phi'_i) = \frac{1}{\sin \beta + \sin \alpha \cos \zeta (1 - \cos \phi'_i)}. \quad (\text{C.5})$$

If r_i is a value so that $\psi_{\text{POL}}(\phi_i) = \psi_{\text{BCW}}(\phi_i)$, (r_i may characterize the true emission height at the phase ϕ_i), then by taking the analogy from Eq. (C.1) we can equate

$$F_1(\phi'_i) = \frac{3r_i}{r_{\text{LC}}} \frac{\sin \zeta}{\sin \beta + \sin \alpha \cos \zeta (1 - \cos \phi'_i)}. \quad (\text{C.6})$$

Then by substituting Eq. (C.6) into (C.3), we get

$$r = \sum_i^N r_i \frac{F^2(\phi'_i)}{\sigma_{\tan \psi}^2(\phi'_i)} \bigg/ \sum_i^N \frac{F^2(\phi'_i)}{\sigma_{\tan \psi}^2(\phi'_i)}. \quad (\text{C.7})$$

Within the bracketed region the small angle approximation for ϕ'_i can be used so that we can re-write expression (C.7) as

$$r \approx \sum_i^N r_i \frac{1}{\sigma_{\tan \psi}^2(\phi'_i)} \bigg/ \sum_i^N \frac{1}{\sigma_{\tan \psi}^2(\phi'_i)}, \quad (\text{C.8})$$

or, by using $\delta\phi'_{\text{PPAIP}} = 2r/r_{\text{LC}}$ and $\delta\phi'_{i(\text{shift})} = 2r_i/r_{\text{LC}}$ we can write

$$\delta\phi'_{\text{PPAIP}} \approx \sum_i^N \delta\phi'_{i(\text{shift})} \frac{1}{\sigma_{\tan \psi}^2(\phi'_i)} \bigg/ \sum_i^N \frac{1}{\sigma_{\tan \psi}^2(\phi'_i)}. \quad (\text{C.9})$$

These expressions (C.8) and (C.9) show that the BCW fit of the PPA data is a weighted average of the emission heights r_i of each data point. If some of the data points are corrupted by the adjacent conals, then the true linear polarization due to the core alone should be less than the observed. Hence it implies that the true PPA value corresponding to the pure core contribution should be slightly different from the observed PPA, which has a small mixture of contribution from adjacent conal component. An approximate method to estimate this error in the PPA ($\Delta\Psi$) due to the ‘‘contamination’’ of the adjacent core is explained in a previous section. Hence the new weight factors are to be defined as

$$\sigma_{\text{TOTAL}}(\phi'_i) = \sqrt{\sigma_{\tan \psi}^2(\phi'_i) + \tan^2[\Delta\Psi_{\text{cone}}(\phi'_i)]},$$

which takes into account the ‘‘contamination’’ of the core due to the adjacent cones. Thus we find

$$r^{\text{pure}} \simeq \frac{\sum_i^N r_i \frac{1}{\sigma_{\text{TOTAL}}^2(\phi'_i)}}{\sum_i^N \frac{1}{\sigma_{\text{TOTAL}}^2(\phi'_i)}} \quad (\text{C.10})$$

and

$$\delta\phi'_{\text{PPAIP}}^{\text{pure}} \simeq \frac{\sum_i^N \delta\phi'_{\text{shift}} \frac{1}{\sigma_{\text{TOTAL}}^2(\phi'_i)}}{\sum_i^N \frac{1}{\sigma_{\text{TOTAL}}^2(\phi'_i)}} \quad (\text{C.11})$$

using the expressions (C.8) and (C.9). In principle, r^{pure} and $\delta\phi'_{\text{PPAIP}}^{\text{pure}}$ characterize the values of emission height and the corresponding phase shift of the PPAIP found for the core region after correcting for the conal contamination. The error induced in locating the PPAIP due to the adjacent conal contamination can be given as $\Delta\delta\phi'_{\text{PPAIP}} = |\delta\phi'_{\text{PPAIP}}^{\text{pure}} - \delta\phi'_{\text{PPAIP}}|$. Hence the improved value of the phase location of PPAIP can be expressed as

$$\delta\phi'_{\text{PPAIP}} \pm \sqrt{\text{Error}(\delta\phi'_{\text{PPAIP}})_{\text{fit}}^2 + \Delta\delta\phi'_{\text{PPAIP}}^2}, \quad (\text{C.12})$$

where $\text{Error}(\delta\phi'_{\text{PPAIP}})_{\text{fit}}$ is the 1σ confidence interval for the $\delta\phi'_{\text{PPAIP}}$ obtained from the BCW91 fit without invoking the correction for conal contamination.

In the actual fitting procedure we used the form of χ^2 as given in Appendix A. We estimated $|\Delta\delta\phi'_{\text{PPAIP}}|$ for the profiles, and the values of $\delta\phi'_{\text{PPAIP}}$ (Table 1) were attributed with an error factor as given by Eq. (C.12). A set of weights are found in the form of $\sigma_{\text{TOTAL}} = \sqrt{\sigma_{\psi}^2 + \Delta\Psi_{\text{cone}}^2}$. The BCW91 model is fitted within the bracketed region after (1) weighting the data with weights σ_{ψ} and (2) again by weighting the data with weights σ_{TOTAL} . The case (1) will yield the phase shift for the PPAIP, while the case (2) should yield the phase shift for the PPAIP with reduced weights to the PPA points where the conal contributions are present. The difference in the phase shifts found by case (1)

and (2) should characterize the extra increment (decrement) in core emission height due to the adjacent conal contributions. The square of this phase shift difference is added with the squared error of the PPAIP phase shift, and the square root of this sum will give the improved error factor for the core emission height. This improved error factor will take into account the error induced in the estimation of the PPAIP in the bracketed region due to the adjacent conal contribution.

References

- Blaskiewicz, M., Coders, J. M., & Wasserman, I. 1991, *ApJ*, 370, 643 (BCW91)
Cordes, J. M. 1978, *ApJ*, 222, 1006
Dyks, J. 2008, *MNRAS*, 391, 859
Dyks, J., & Harding, A. K. 2004, *ApJ*, 614, 869
Dyks, J., Rudak, B., & Harding, A. K. 2004, *ApJ*, 607, 939 (DRH04)
Everette, J. E., & Weisberg, J. M. 2001, *ApJ*, 341, 357
Gangadhara, R. T. 2004, *ApJ*, 609, 335 (G04)
Gangadhara, R. T. 2005, *ApJ*, 628, 930 (G05)
Gangadhara, R. T., & Gupta, Y. 2001, *ApJ*, 555, 31 (GG01)
Gil, J. A., & Kijak, J. 1993, *A&A*, 273, 563
Gupta, Y., & Gangadhara, R. T. 2003, *ApJ*, 584, 41 (GG03)
Hibschman, J. A., & Arons, J. 2001, *ApJ*, 546, 382
Hoensbroech, von A., & Xilouris, K. M. 1997, *A&A*, 324, 981
Johnston, S., & Weisberg, J. M. 2006, *MNRAS*, 368, 1856
Kijak, J., & Gil, J. 2003, *A&A*, 397, 969
Kramer, M., Wielebinski, R., Jessner, A., Gil, J. A., & Seiradakis, J. H. 1994, *A&AS*, 107, 515
Krzyszowski, K., Mitca, D., Gupta, Y., et al. 2009, *MNRAS*, 393, 1617
Lyne, A. G., & Manchester, R. N. 1988, *MNRAS*, 234, 477
Mitra, D., & Deshpande, A. A. 1999, *A&A*, 346, 906
Mitra, D., & Li, X. H. 2004, *A&A*, 421, 215 (ML04)
Naghizadeh-Khouei, J., & Clarke, D. 1993, *A&A*, 274, 968
Rankin, J. M. 1983a, *ApJ*, 274, 333
Rankin, J. M. 1983b, *ApJ*, 274, 359
Rankin, J. M. 1990, *ApJ*, 352, 247
Rankin, J. M. 1993, *ApJS*, 85, 145
Ruderman, M. A., & Sutherland, P. G. 1975, *ApJ*, 196, 51
Shitov, Yu. P. 1983, *SVA*, 27, 314
Zhang, H., Qiao, G. J., Han, J. L., Lee, K. J., & Wang, H. G. 2007, *A&A*, 465, 525